Photodissociation Dynamics of Cumene Hydroperoxide at 248 and 193 nm

Seung Keun Shin, Soon Ok Park, Young Sik Choi,† and Hong Lae Kim*

Department of Chemistry, Kangwon National University, Chuncheon 200-701, Korea

Chan Ryang Park

Department of Chemistry, College of Natural Sciences, Kookmin University, Seoul 136-702, Korea

Received: June 19, 2001; In Final Form: August 30, 2001

Photodissociation dynamics of cumene hydroperoxide at 248 and 193 nm producing $(C_6H_5)(CH_3)_2CO$ (CumO) and OH fragments has been investigated by measuring laser induced fluorescence spectra of the OH fragments, which are produced exclusively in the ground electronic state. The measured energy distributions among the fragments are $f_r(OH) = 0.03$, $f_t = 0.49$, $f_{int}(CumO) = 0.48$ and $f_r(OH) = 0.03$, $f_t = 0.18$, $f_{int}(CumO) = 0.79$ at 248 and 193 nm, respectively, and negligible vibrational excitation in OH was observed at both wavelengths. At 248 nm, slightly negative $\mu-v$ and positive $v-J$ vector correlations were observed by analyzing the Doppler profiles of the rotationally resolved OH spectra, whereas no vector correlations were observed at 193 nm. From the measurements, detailed photodissociation dynamics of cumene hydroperoxide is discussed compared to the case of *tert*-butyl hydroperoxide previously studied.

Introduction

Studies of molecular photodissociation dynamics are of fundamental importance to investigate electronic structures of molecules because the process is governed by the excited state and potential energy surfaces along the reaction coordinate. The detailed dynamics of the process can be understood by measuring energies and certain vector properties of the system. These physical properties of the system can be measured precisely from optical spectra in favorable cases where the photofragments absorb and/or emit radiation in an easily accessible spectral region. The Doppler broadened absorption or emission spectra of the photofragments by polarized photolysis and probe lights provide information on the energy distribution among various degrees of freedom of the fragments as well as directions of the transition dipole moment, recoil velocity and angular momenta of the fragments.[1−3] From the measurements, the excited state and the potential energy surfaces along the reaction coordinate can be explored.

Spectroscopic transitions in molecules to the repulsive part of the potential energy surface generally result in continuous spectra. One can theoretically determine the energies of the excited states and describe the nature of the transitions by ab initio calculations. When the dissociation starts from the repulsive potential surface (direct dissociation), the angular distribution of the fragments is especially important among many experimental observables in determining the nature of the excited state. Maximum absorption of the dissociating light by the molecule takes place when the transition dipole moment of the molecule lies along the electric vector of the linearly polarized dissociating light. Thus, the angular distribution of the recoiling fragments measured relative to the electric vector of the dissociating light in the laboratory frame reveals the direction of the transition dipole moment of the molecule in the molecular frame. From the direction of the transition dipole moment, the symmetry of the excited state can be identified according to proper selection rules.

However, in the case of indirect dissociation when intersystem crossing or internal conversion between the electronic states takes place before the dissociation, the dissociation would be slow compared to the molecular rotational period. As a result, the directional memory upon absorption should be lost, resulting in little or no correlation between the direction of the electric vector of the photolysis light and the recoil velocity of the fragments, except for certain cases such as dissociation of Na_2 from a quasibound level ($\tau \sim 1.6$ ns) in the B state where the translational anisotropy is preserved.[4] However, even in the case of slow dissociation, whether statistical theories such as the RRKM theory can be applied to the dissociation dynamics is still interesting because, although complicated, the dissociation dynamics can provide information on the potential energy surfaces.

The Doppler profiles in polarized absorption and emission spectra of molecules have been thoroughly analyzed by Herschbach and Zare.[5] The line shapes of the spectra are determined by the coupling of rotational and translational motion of the molecules. Thus, the Doppler broadened spectra of the photofragments provide relationships between the velocities and the rotational angular momenta of the fragments. The Doppler spectroscopic technique is limited by the resolution of the spectra. The translational energies of the fragments should be large enough to provide broad spectroscopic transitions, whereas the individual rotational transition should also be resolved in the spectra under the given resolution. A commercial dye laser currently available typically provides 0.04 cm^{-1} bandwidth in the visible region, and various laser spectroscopic techniques such as laser-induced fluorescence (LIF) have been widely used to obtain the high-resolution spectra of the photofragments.

Studies of the photodissociation of organic peroxides by irradiation of UV light have been reported for many years. In particular, the photodissociation of H_2O_2 in the first UV

* Corresponding author. E-mail: hlkim@cc.kangwon.ac.kr
† Current address: Department of Chemistry, Inha University, Incheon 402-751, Korea

10.1021/jp012312+ CCC: $20.00
Published on Web 10/09/2001

absorption band has been thoroughly studied.[6−8] The transition is assigned as $\sigma^* \leftarrow n$, whose transition dipole moment lies perpendicular to the O−O bond axis. The complete vector correlations were measured, from which the detailed dynamics of the dissociation process at 266 nm was analyzed. The photodissociation of $(CH_3)_3COOH$ is another example of studying the dynamics by applying the Doppler spectroscopic technique. In addition, it is interesting to study the effect of alkyl substitution in H_2O_2 on the dissociation dynamics because the symmetry is lower and the substituted group is relatively heavy. $(CH_3)_3COOH$ is dissociated into *tert*-butoxy (t-BuO) and OH radicals upon irradiation of the UV light. In the studies of photodissociation at 248 nm, slightly negative $\mu-v$ and slightly positive $v-J$ correlation at high J were observed.[9] In the case of H_2O_2 at 266 nm, a negative $\mu-v$ correlation ($\beta = -1$) was reported.[6] The perpendicular transition in this spectral region results in the negative limiting value of the $\mu-v$ correlation in H_2O_2 but the relatively large t-BuO group affects the dynamics of the dissociation, resulting in the smaller translational anisotropy parameter β in the case of $(CH_3)_3COOH$. At 193 nm, it was found that the transition leads to a mixture of the A and B states in H_2O_2, and the dynamics was studied by measuring the vector correlations of the OH fragments.[7,8] The dissociation occurs directly from the repulsive A and B states, and most of the available energy has been found to be distributed in the product translation (∼90%). In the case of $(CH_3)_3COOH$, a similar transition to the A and B states at 193 nm and the direct dissociation were suggested by studying the vector correlations of the OH fragments.[10] On the other hand, Crim and co-workers studied the vibration-mediated photodissociation via the fifth overtone excitation of the OH stretching vibration of $(CH_3)_3$-COOH.[11] They found large internal excitation in the t-BuO group, contrary to the direct dissociation from the repulsive state.

The absorption spectra of cumene hydroperoxide (CumOOH), which is the molecule having one phenyl group instead of a methyl group in *tert*-butyl hydroperoxide, have not yet been reported. However, the characteristic $\sigma^* \leftarrow n$ transition due to the O−O bond, as in peroxides, and the $\pi^* \leftarrow \pi$ transition in the phenyl group would be expected in the UV. In fact, the continuous absorption band around 190 nm appears in the spectra of cumene, which can be assigned as the similar, vibronically allowed B ← X transition in benzene.[12] Thus, the dissociation dynamics would be very different at the photolysis wavelengths in this spectral region.

The photodissociation dynamics of cumene hydroperoxide at 248 and 193 nm was studied by measuring the laser-induced fluorescence spectra of the OH fragments. By analyzing the Doppler profiles of the spectra, the energy distribution and the vector correlations of the fragments were obtained.

Experimental Section

The experiment was performed in a flow cell with the conventional pump−probe geometry. The cell is a cube made of stainless steel with four arms in which baffles are placed to minimize scattered light. The cell was evacuated at a pressure of about 10^{-3} Torr, and the gaseous sample was continuously flowed at a sample pressure of about 20 mTorr. The cumene hydroperoxide, purchased from Aldrich (90% purity), was pumped through a glass sample cell for at least 4 h until it reached a concentration of higher than 95% before use.

The 193 or 248 nm dissociating light was obtained from an ArF or KrF excimer laser (Lambda Physik Lextra 50), respectively, whose output was linearly polarized with a stack of quartz plates at a Brewster angle. The horizontally polarized probe light was a frequency-doubled output of a dye laser (Lumonics HD-500) pumped by the second harmonic of an Nd:YAG laser (Lumonics YM-800). The two laser beams were temporally separated by about 50 ns. The 50 ns delay time between the pump and probe light and 20 mTorr sample pressure should ensure a nascent product energy distribution. The laser-induced fluorescence (LIF) spectra of the OH fragments were measured using the A−X transition in UV. The 0−0 transition of OH was excited, and the resulting total fluorescence was probed through a filter (UG-11). The power of the probe laser light was kept as low as possible (typically 20 μJ/pulse) to avoid saturation and to minimize the scattered radiation. The scattered radiation was also cut off through baffles, which were placed in the arms attached to the cell. To measure the Doppler profiles of the spectra, several rotational transitions were probed under high resolution. The bandwidth of the probe laser light is 0.07 cm^{-1} in the visible, which was measured by the line width of the rotationally resolved gaseous I_2 spectra at ambient temperature. The horizontally polarized dissociating and probe laser beams were collinearly counterpropagated or introduced at a right angle to the cell to obtain two different experimental geometries. The former geometry provides $\epsilon_d \perp k_p$ and $\epsilon_d \parallel \epsilon_p$, while the latter provides $\epsilon_d \parallel k_p$ and $\epsilon_d \perp \epsilon_p$, where ϵ_d and ϵ_p are the directions of the electric vectors of the dissociating and probe lights and k_p is the propagation direction of the probe light, respectively.

The laser-induced fluorescence was detected through a collection lens by a PMT (Hamamatsu R212UH) whose direction of view was at a right angle to the two laser beams, and the detected signal was fed to a boxcar averager. The powers of the dissociating and probe lights were measured separately, and the detected signal was corrected for variation of the laser powers. A signal processor digitized the signal that was stored and processed in a PC.

Results and Analyses

A portion of the LIF spectra of the OH fragments produced from the photodissociation of cumene hydroperoxide at 248 and 193 nm is presented in Figure 1. In the spectra, individual rotational transitions in the 0−0 band of the A−X transition are resolved and assigned according to Dieke and Crosswhite.[13] The rotational transitions from the 1−1 band region were measured, but no appreciable intensities exceeded the noise in the spectra. The rotational transitions from the higher vibrational states of OH could not be measured from diagonal transitions such as 2−2 and 3−3 bands due to extensive predissociation from the higher vibrational states in the A state. However, since no appreciable slow speed components corresponding to the higher vibrational states of OH were observed in the Doppler profiles, it was concluded that the population of OH in the higher vibrational states is negligible. Then, the rotational population distributions, the spin−orbit population ratios between the $^2\Pi_{1/2}$ and $^2\Pi_{3/2}$ states of OH, and the Λ-doublet distributions were measured from the spectra. The translational energies and the vector correlations were also measured from the analysis of the Doppler profiles of the spectra.

A. Photodissociation at 248 nm. The rotational population distribution which peaks at the rotational quantum number $N = 4,5$ and extends to $N = 12$ was obtained from the measured spectra by using the reported Einstein B coefficients (Figure 2).[14] From the distribution, the average rotational energy of OH was found to be about 840 cm^{-1}. Correlations of rotation with translational motion have been thoroughly analyzed by Dixon,[15] and the anisotropy is defined by a number of bipolar moments

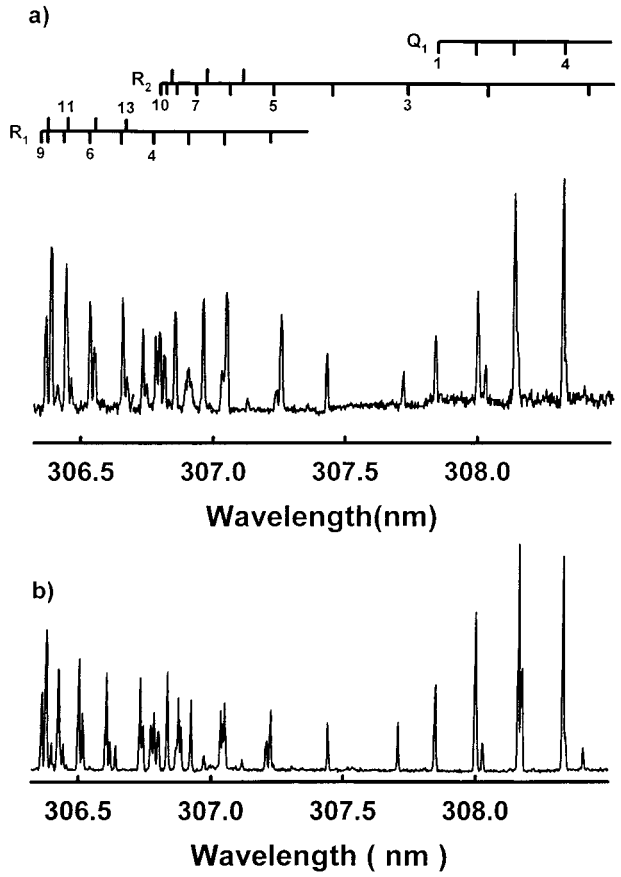

Figure 1. Portions of the LIF excitation spectra of OH produced from the photodissociation of cumene hydroperoxide (a) at 248 nm and (b) at 193 nm employing the 0−0, A←X transition. The assignments are from ref 13.

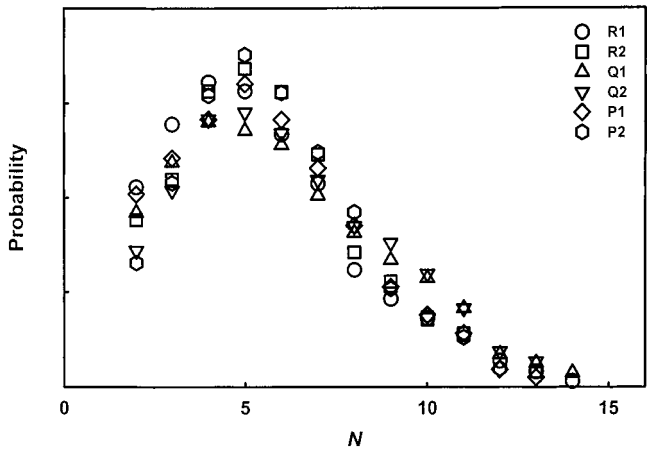

Figure 2. Rotational population distribution of OH produced from the photodissociation of cumene hydroperoxide at 248 nm.

of the translational and rotational angular distributions. The Doppler broadened line shape in the LIF spectra of the photofragments depends on the rotational alignment, the polarizations of the photolysis and probe lights, the excitation-detection geometries, and the rotational branch transitions probed. The generalized line shape functions are then given by

$$g(\chi_D) = \frac{1}{2\nu_D}[g_0 + g_2P_2(\chi_D) + g_4P_4(\chi_D) + g_6P_6(\chi_D)]$$

where χ_D and ν_D are the relative and the maximum Doppler shift, respectively, and P_x are the even-order Legendre polynomials. The Legendre polynomials of the fourth and sixth order are often neglected since the contribution of these high order terms to the Doppler profiles is small compared to the experimental errors. The multipliers, g_x, in the above equation are the linear combination of the bipolar moments, β_0^k, which are given by

$$g_0 = b_0 + b_1\beta_0^2(02)$$

$$g_2 = b_2\beta_0^2(20) + b_3\beta_0^0(22) + b_4\beta_0^2(22)$$

where b_x can be calculated from the excitation-detection geometries and the angular momentum coupling factors defined by Dixon.[15] In this experiment, the two different excitation-detection geometries described in the Experimental Section were employed, and the corresponding b values were obtained for the different rotational branch transitions.[16] The bipolar moments, β_0^2 (02), β_0^2 (20), β_0^0 (22), β_0^2 (22) represent the rotational alignment, $\beta_{\mu J}$, translational anisotropy, $\beta_{\mu\nu}$ (= $2\beta_0^2(20)$), ν−J, and $\mu-\nu-J$ photofragment vector correlations, respectively. The experimental Doppler profiles are fitted by the equation

$$g(\chi_D) = \frac{1}{2\nu_D}[1 + \beta_{eff}P_2(\theta)P_2(\chi_D)]$$

where θ is the angle between the recoil velocity and the probe direction and

$$\beta_{eff} = [b_2\beta_0^2(20) + b_3\beta_0^0(22) + b_4\beta_0^2(22)]/g_0P_2(\theta)$$

From the least-squares fit of the observed profiles by the above equation, the four bipolar moments can be calculated by solving the linear equations.

The Doppler-resolved spectra were measured for the P_1 and Q_1 or R_1 and Q_1 rotational branch transitions for the rotational quantum numbers N = 4,5,6,9,10,12,14 which are well separated from other transitions. In Figure 3, typical Doppler broadened LIF spectra for N = 14 are presented. Since the CumO fragments should have internal energy distributions, the OH fragments should have corresponding speed distributions. However, the internal energy distributions of the CumO fragments were not measured in this experiment. Thus, the measured profiles were fitted assuming Gaussian speed distribution with various widths. To find the best fits, the following procedures were employed. First, the best fit was found to the observed profile of one rotational branch transition varying β_{eff}, the average speed, and the width of the speed distribution. The measured average speed and the width for the best fit are 3400 m/s and 1200 m/s for N = 14, respectively. This speed corresponds to the average translational energy of 12 570 cm^{-1}, from which the center of mass translational energy was calculated to be 14 150 cm^{-1}. Then, for the profiles of the different rotational branch transitions under different experimental geometries at the same N, the best fit was obtained by just varying β_{eff}. From the measured β_{eff} values for the same N, the bipolar moments were calculated by solving the linear equations. The calculated bipolar moments for different N are presented in Figure 4. In the figure, the negative translational anisotropy parameter ($\beta_{\mu\nu}$ = −0.1) indicates that the OH fragments should be essentially ejected perpendicular to the transition dipole moment of the parent molecule, although the value is far from the limiting value of −1. The positive increasing ν−J correlation with increasing N implies more parallel orientation of the rotational angular momentum J_{OH} to the recoil velocity v_{OH} (out-of-plane dis-

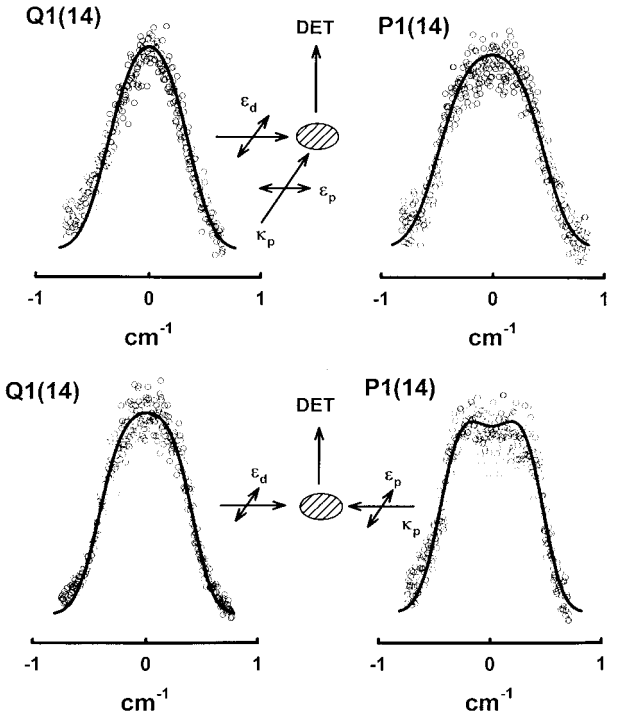

Figure 3. Doppler profiles of the rotationally resolved spectra of OH at the rotational quantum number 14 under two different experimental geometries described in the Experimental Section. Smooth curves are the best fits to the equation given in the text.

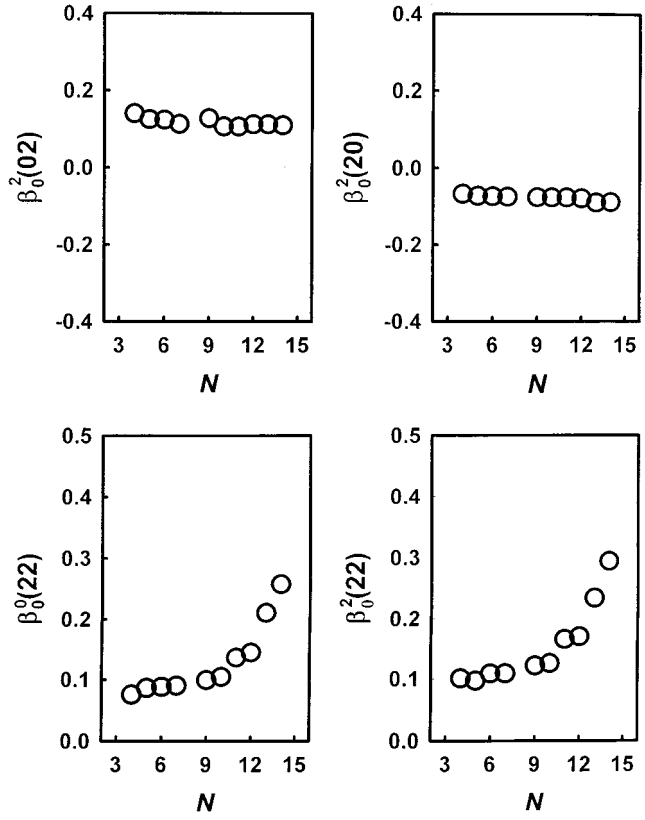

Figure 4. Vector correlations as a function of the rotational quantum numbers by solving the linear equations (see the text).

sociation). In addition, a slightly positive $\mu-J$ and positive $\mu-v-J$ correlations were also observed.

In Figures 5 and 6, the Λ-doublet distribution and $^2\Pi_{1/2}$ $(N+1)/^2\Pi_{3/2}N$ ratio in the OH fragment are presented as a function of N while the statistical ratio is unity. The statistical

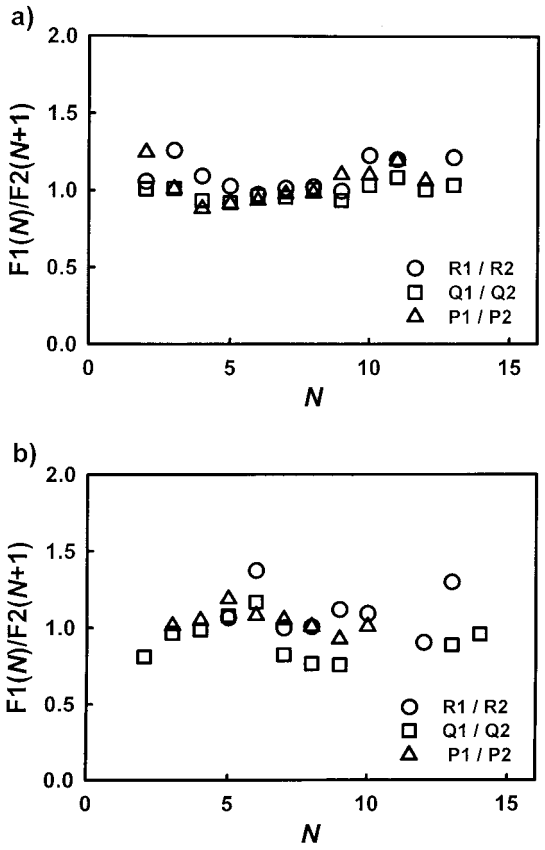

Figure 5. F1/F2 ratios of OH as a function of the rotational quantum numbers from the measured LIF spectra in Figure 1: (a) 248 nm, (b) 193 nm.

population distribution between the two spin−orbit states was observed. However, the measured distribution shows that the Π^- Λ-doublet state is preferentially populated at high N, which suggests that the OH fragments tend to rotate in the plane perpendicular to the dissociating bond axis.

B. Photodissociation at 193 nm. In Figure 7, the rotational population distribution of OH produced from the 193 nm photodissociation is presented. The distribution peaks around at $N = 5,6$ and extends up to $N = 18$, from which the average rotational energy was obtained to be about 1300 cm^{-1}. For individual rotational transition, the Doppler profiles were obtained under different experimental geometries. However, the observed profiles are essentially the same for all geometries, contrary to the 248 nm photodissociation case. It was then concluded that there should be no polarization dependence. However, the widths of the profiles, which are Gaussian, are large enough to measure the average translational energy of the OH fragments from the second moment of the distribution after deconvolution of the laser line width. The measured average translational energy release is 7460 cm^{-1}.

Discussion

A. Photodissociation at 248 nm. The UV spectrum of Cumene hydroperoxide shows continuous, weak absorption starting from around 250 nm and structured, strong absorption near 193 nm (Figure 8), although the structured absorption is not clearly identified as being due either to vibrational transitions or due to different electronic transitions. In any case, as in *tert*-butyl hydroperoxide, the continuous absorption at 248 nm could be identified as the $n \rightarrow \sigma^*$ transition along the O−O bond to the lowest repulsive A state.[9] Thus, similar to *tert*-butyl

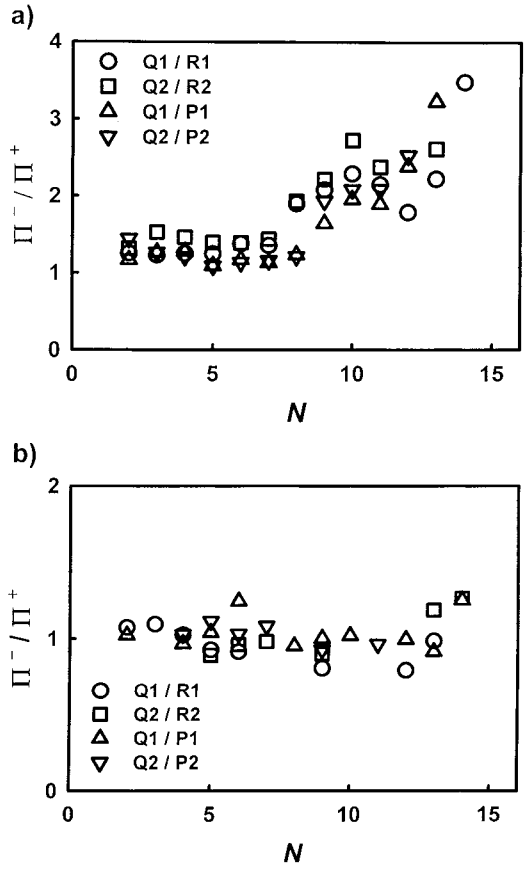

Figure 6. Λ-doublet distribution of OH as a function of the rotational quantum numbers from the measured LIF spectra in Figure 1: (a) 248 nm, (b) 193 nm.

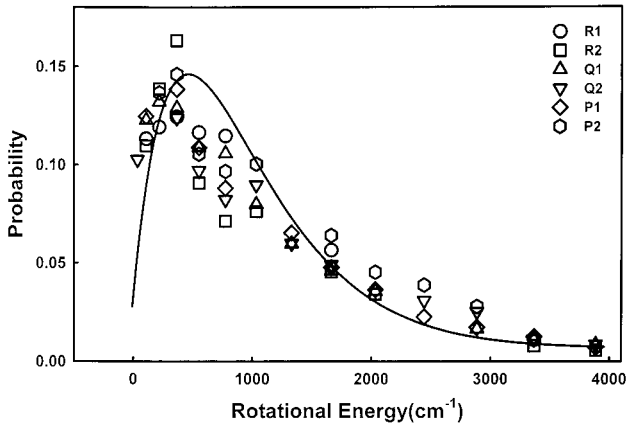

Figure 7. Rotational population distribution of OH produced from the photodissociation of cumene hydroperoxide at 193 nm. Symbols are from the experiment and the smooth curve is from the prior calculation (see text).

hydroperoxide, the photodissociation dynamics of cumene hydroperoxide can be understood as the electronic transition at 248 nm to this repulsive surface, which results in the direct, impulsive dissociation. In H_2O_2, the direction of the transition dipole moment of the lowest electronic transition to the repulsive A state is perpendicular to the dissociating O−O bond (perpendicular transition). Although the methyl and phenyl substitution to H_2O_2 lowers the overall symmetry of the parent molecule and hence the direction of the transition dipole moment cannot be clearly identified, the transition at this wavelength could be still assumed to be essentially perpendicular. The measured negative translational anisotropy parameter of −0.1 is the result

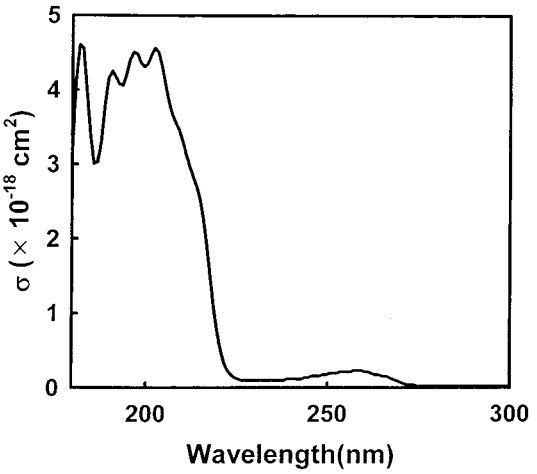

Figure 8. UV absorption spectra of cumene hydroperoxide in the gas phase using the SCINCO S-2180 spectrophotometer at a sample pressure of 1.6 Torr and 10 cm cell path length.

TABLE 1: Fraction of the Available Energy Distributed among the Products Produced from the Photodissociation of $(C_6H_5)(CH_3)_2COOH$

$E_{av}(cm^{-1})^a$	$\langle f_t \rangle$	$\langle f_r(OH) \rangle$	$\langle f_v(OH) \rangle$	$\langle f_{int}((C_6H_5)(CH_3)_2CO) \rangle$
at 193 nm				
40,530	0.18	0.032	<0.01[b]	0.79
at 248 nm				
29,040	0.49	0.029	<0.01[b]	0.48
impulsive model	0.53	0.028		

[a] $E_{av} = h\nu + E_{int}((C_6H_5)(CH_3)_2COOH \text{ at } 300K) - D_0((C_6H_5)(CH_3)_2CO-OH)$. [b] Approximated from the noise in the spectra.

of this perpendicular transition, although the limiting value is −1 for the pure perpendicular transition. In fact, the translational anisotropy parameter of −1 was observed for the dissociation of H_2O_2 from the repulsive A state.[6] The deviation of the translational anisotropy parameter from the limiting value might be due to molecular rotation of the parent molecule during the dissociation and/or to some dynamical effects. However, judging from the repulsive nature of the dissociating surface and the slow rotational period of the parent molecule on the order of picoseconds, it is unlikely that the molecular rotation reduces the translational anisotropy. Thus, as Simons and co-workers pointed out in the dissociation of *tert*-butyl hydroperoxide,[9] it is suggested that the bending torque at the impulse would deflect the fragment OH out of the recoil direction, which will substantially reduce the translational anisotropy.

The dissociation energy of cumene hydroperoxide has not yet been reported. Thus, the dissociation energy was obtained by ab initio calculations using the GAUSSIAN program package.[17] The B3LYP calculations were performed using the 6-31G(2df, 3pd) basis set, which provides the dissociation energy of 36.8 kcal/mol. To estimate the accuracy of the calculation, the same calculation was carried out for the dissociation energy of *tert*-butyl hydroperoxide. The dissociation energy obtained from the calculation is 40.4 kcal/mol, whose value taken from the literature is 40. 8 kcal/mol.[9] Thus, the obtained dissociation energy of cumene hydroperoxide from the calculation should have accuracy similar to that in the case of *tert*-butyl hydroperoxide. Then the available energy, which can be distributed among the fragments from the photodissociation at 248 nm, is 29 040 cm^{-1} and the measured fractions of the available energy in the products are listed in Table 1. The measured energy partitioning in the fragments is well explained by the impulsive dissociation model, which assumes direct and

fast dissociation.[18] In the model, the initial excitation is expected to turn on the impulsive force between the departing O−O atoms. The linear momentum of the atoms is then transferred to the fragments, and the average translational and internal energies of the fragments are calculated based on the momentum and energy conservation. The measured energy distribution implies that the dissociation is direct and fast from the repulsive surfaces as mentioned above. However, a recent quantum dynamical calculation of the photodissociation of H_2O_2 shows that the rotational population distribution of the OH fragment should be Gaussian-like, with a tail at high N due to bending and torsional couplings.[19,20] If more torsional couplings are taken into account, the distribution shows more tailing to the high N side. The ab initio calculations of the equilibrium geometry of H_2O_2 indicate the dihedral angle of 120° at the trans planar geometry, and the barrier for corresponding cis−trans configuration change is 386 cm^{-1}.[21] The alkyl substitution slightly opens the dihedral angle in CH_3OOH and greatly reduces the barrier($\sim$80 cm^{-1}). Assuming a similar trend in methyl and phenyl substitution in cumene hydroperoxide, the barrier is expected to be much lower than the zero point energy of the OH torsional motion. Thus, the wide angle torsional motion of the parent molecule is likely transformed to the fragment OH rotational motion upon dissociation, and the rotational population distribution observed in this experiment reflects the importance of the parent torsional motion, especially at high N. The fact that the parent torsional motion should play an important role in the OH fragment rotation is ascertained by the positive $v-J$ vector correlation measured in this experiment.

Coupling between rotation and translational motion can be analyzed by the shape of the Doppler profiles of the spectra of the OH fragment. Since the $v-J$ correlation is developed at the moment of dissociation, it can be observed even in the isotropic dissociation. If the source of the fragment OH rotation is the bending torque or the impulsive force, the rotational angular momentum should be aligned perpendicular to the recoil direction. In this case, the negative $v-J$ correlation is expected. However, if the parent torsional motion is the source of the OH rotation, the rotational angular momentum should be aligned parallel to the recoil direction and hence the positive $v-J$ correlation would be observed. The $v-J$ correlation measured in this experiment is positive and increases as N increases, implying again that the parent torsional motion plays the important role in the fragment OH rotation.

In a diatomic molecule with a singly occupied p_π orbital such as OH produced in this experiment, coupling between the electronic angular momentum and nuclear rotation splits the two degenerate states of $\Lambda = \pm 1$, the orbital angular momentum projecting to the internuclear axis.[22] In the limit of high rotation, the p_π orbital is approximated as a lobe aligned perpendicular to the plane of rotation (Π^-, the lower Λ state) or a lobe in the plane of rotation (Π^+, the upper Λ state). According to the parity selection rule, the Q-branch rotational transition is induced from the Π^- state, while the R- and P-branch transitions are induced from the Π^+ state in the electronic transition. Thus, the specific Λ-doublet population can be experimentally measured in the spectra. The distribution between the two Λ-doublet states of OH produced in the photodissociation depends on the correlation on the p_π orbital of the OH fragment with the orbitals of the parent molecule and how the p_π orbital is generated upon dissociation; that is, the mechanism of the dissociation process. The measured Λ-doublet distribution at 248 nm shows a propensity in the Π^- state, and the propensity is increased as N is increased, indicating that the unpaired p_π orbital of the OH fragment is aligned more perpendicular to the plane of rotation. The higher propensity in the Π^- state of OH recoiling with higher rotational angular momentum indicates that the p_π orbital lobe of the OH fragment conserves some of the orientations of the corresponding p_π orbital in the excited parent molecule just before dissociation and reflects the importance of the angular motion such as torsion on the excited surfaces.

B. Photodissociation at 193 nm. The experimental results clearly differ from the results of the photodisssociation at 248 nm, which implies different dissociation pathways at 193 nm. Contrary to the 248 nm dissociation case, no polarization dependence and less translational energy release were observed, although the photon energy at 193 nm is larger, which implies no direct, impulsive dissociation. One might think at a glance of an indirect dissociation from the ground state as a result of internal conversion. As can be seen in the absorption spectra, the huge absorption band around 193 nm might be assigned as the $\pi \rightarrow \pi^*$ transition due to the phenyl group. Then, the initial transition to the excited state followed by the internal conversion to the ground state may result in slow dissociation. In this case, the energy partitioning can be estimated by some statistical theories such as a prior theory.[23,24] It is assumed in the prior model that the available energy should be randomly distributed in the products before the dissociation and hence that it should be distributed among all product degrees of freedom with equal probability. Thus, the translational energy is proportional to the number of accessible quantum states among the products at the energy $E = E_{av} - E_t$. The vibrational frequencies of the CumO radical were calculated by the ab initio calculation using the 6-31G* basis set, and the calculations were performed under the HF level using the GAUSSIAN program package.[17] The translational energy distribution was obtained by directly counting the number of vibrational states and ignoring the rotational energy of the CumO radical because the rotational energy of CumO is very small. From the distribution, the average translational energy of OH was obtained to be 990 cm^{-1}, which is far smaller than the translational energy measured in this experiment (7460 cm^{-1}). The translational energy distribution was also calculated by the simple formula given by Zamir and Levine,[24] which is

$$P(f_t|E) = f_t^{1/2}(1 - f_t)^{s+5/2}$$

where f_t is the fraction of the translational energy and s is the number of vibrational degrees of freedom in the CumO radical. From this calculation, the average translational energy of 950 cm^{-1} was again obtained for $s = 59$. The experimentally measured average translational energy of 7460 cm^{-1} could never be obtained, even for very low s value (for example, 1760 cm^{-1} for $s = 10$), implying no energy randomization in the dissociation process. Assuming the statistical dissociation, the rate constant was calculated by the RRKM theory. The vibrational frequencies of the cumene hydroperoxide at the transition state were calculated by the same ab initio calculation assuming twice the O−O bond length as that of the parent molecule. The calculated rate constant is 9.5×10^6 s^{-1}, which is very slow for the products to be detected in the present nanosecond time scale experiment. Therefore, it is concluded from the above discussion that the dissociation should not statistically take place in the ground electronic state.

Another possible dissociation pathway is the indirect dissociation from the repulsive part of the potential energy surfaces along the O−O bond resulting from curve crossing. In this case, an appreciable amount of an energy barrier may exist in the exit channel, although the barrier height may depend on the

position of the curve crossing. In fact, it has been suggested that at 193 nm the electronic transition reaches the repulsive A and B states, and direct dissociation was observed in H_2O_2 and *tert*-butyl hydroperoxide by measuring the vector correlations.[8,10] However, in cumene hydroperoxide, no polarization dependence suggests that the dominant transition at 193 nm should be $\pi \rightarrow \pi^*$ in the phenyl group rather than the $n \rightarrow \sigma^*$ transition along the O−O bond. One might think that the energy transfer from a strong transition dipole (phenyl) to a weak dipole (O−O bond) would induce the O−O bond cleavage. This so-called Forster-type transfer may be a specific example of a curve crossing. Then, if we assume that the parent molecule spends some time such as several vibrational periods in the excited singlet surface followed by the curve crossing to the repulsive surface, the energy of the reverse barrier would be transformed into the product translation and the remaining available energy may be statistically distributed among the various product degrees of freedom. This kind of energy partitioning was also observed in the photodissociation of acetaldehyde and acetic acid.[25,26] Thus, the reverse barrier of 6500 cm^{-1} for the dissociation of cumene hydroperoxide at 193 nm is suggested (measured translational energy minus the statistical partitioning of the translational energy from the remaining available energy). Then, the rotational energy distribution was calculated by the same statistical prior model, which well fits the experimentally measured rotational distribution (Figure 7). In summary, the photodissociation of cumene hydroperoxide at 193 nm indirectly takes place from the repulsive part of the electronically excited surface, with the exit channel barrier resulting from the curve crossing from the initially excited singlet surface. In this case, the translational energy release would be more or less invariant with the photon energy. However, to clarify the dissociation mechanism in more detail at this short wavelength, detailed theoretical investigations on the potential energy surfaces would be helpful.

Conclusion

Photodissociation dynamics of cumene hydroperoxide in UV has been investigated by measuring energy partitioning and vector correlations among products. At 248 nm, the $n \rightarrow \sigma^*$ transition leads the molecule to the repulsive part of the potential surface and the direct, impulsive dissociation takes place. However, at 193 nm, the initial $\pi \rightarrow \pi^*$ transition followed by curve crossing to the repulsive part of the potential surface induces the indirect dissociation with the exit channel barrier.

Acknowledgment. This work was financially supported by the Korea Science and Engineering Foundation.

References and Notes

(1) Hall, G. E.; Houston, P. *Ann. Rev. phys. Chem*. **1989**, *375*, 40.

(2) Ashfold, M. N. R.; Baggott, J. E., Eds. *Molecular Photodissociation Dynamics*; Royal Society of Chemistry: London, 1987.

(3) Simons, J. P. *J. Phys. Chem*. **1987**, *91*, 5378.

(4) Gerber, G.; Moeller, R. *Phys. Rev. Lett*. **1985**, *55*, 814.

(5) Zare, R. N.; Herschbach, D. R. *Proc. IEEE*, **1963**, *51*, 173.

(6) Gericke, K−H.; Klee, S.; Comes, H. J.; Dixon, R. N. *J. Chem. Phys*. **1986**, *85*, 4463.

(7) Ondrey, G.; van Veen, N.; Bersohn, R. *J. Chem. Phys*. **1983**, *78*, 3732.

(8) Grunewald, A. U.; Gericke, K−H.; Comes, H. J. *J. Chem. Phys*. **1987**, *87*, 5709.

(9) August, J.; Brouard, M.; Docker, M. P.; Milne, C. J.; Simons, J. P.; Lavi, R.; Rosenwaks, S.; Schwartz-Lavi, D. *J. Phys. Chem*. **1988**, *92*, 5485.

(10) Shin, S. K.; Kim, H. L.; Park, C. R. *J. Phys. Chem. A* **1999**, *103*, 4150.

(11) Likar, M. D.; Baggott, J. E.; Sinha, A.; Ticich, T. M.; Vander Wal, R. L.; Crim, F. F. *J. Chem. Soc., Faraday Trans*. **1988**, *84*, 1483.

(12) Robin, M. B.; *Higher Excited States of Polyatomic Molecules, Vol. II*; Academic Press: New York, 1975.

(13) Dieke, G. H.; Crosswhite, H. M. *J. Quant. Spectrosc. Radiat. Transfer*, **1962**, *2*, 97.

(14) Chidsey, I. L.; Crosely, D. R. *J. Quant. Spectrosc. Radiat. Transfer*, **1980**, *23*, 187.

(15) Dixon, R. N. *J. Chem. Phys*. **1986**, *85*, 1866.

(16) Baek, S. J.; Park, C. R.; Kim, H. L. *J. Photochem. Photobiol. A* **1997**, *104*, 13.

(17) Gaussian 98, Frisch, M. J.; Trucks, G. W.; Schlegel, H. B.; Scuseria, G. E.; Robb, M. A.; Cheeseman, J. R.; Zakrzewski, V. G.; Montgomery, J. A.; Stratmann, R. E.; Burant, J. C.; Dapprich, S.; Millam, J. M.; Daniels, A. D.; Kudin, K. N.; Strain, M. C.; Farkas, O.; Tomasi, J.; Barone, V.; Cossi, M.; Cammi, R.; Mennucci, B.; Pomelli, C.; Adamo, C.; Clifford, S.; Ochterski, J.; Perdersen, G. A.; Ayala, P. Y.; Cui, Q.; Morokuma, K.; Malick, D. K.; Rabuck, A. D.; Raghavachari, K.; Foresman, J. B.; Cioslowski, J.; Ortiz, J. V.; Stefanov, B. B.; Liu, G.; Liashenko, A.; Piskorz, P.; Komaromi, I.; Gomperts, R.; Martin, R. L.; Fox, D. J.; Keith, T.; Al-Laham, M. A.; Peng, C. Y.; Nagayakkara, A.; Gonzales, C,; Challacombe, M.; Gill, P. M. W.; Johnson, B. G.; Chen. W.; Wong, M. W.; Andres, J. L.; Head-Gordon, M.; Replogle, E. S.; Pople, J. A. Gaussian Inc., Pittsburgh PA, 1998.

(18) Tuck, A. F. *J. Chem. Soc., Faraday Trans. II* **1977**, *73*, 689.

(19) Bersohn, R.; Shapiro, M. *J. Chem. Phys*. **1986**, *85*, 1396.

(20) Zhang, D. H.; Zhang, J. Z. H. *J. Chem. Phys*. **1992**, *98*, 6276.

(21) Bair, R. A.; Goddard, W. A., III *J. Am. Chem. Soc*. **1982**, *104*, 2719.

(22) Hanazaki, I. *Chem. Phys. Lett*. **1993**, *201*, 301.

(23) Levine, R. D.; Bernstein, R. B. *Molecular Reaction Dynamics and Chemical Reactivity*; Oxford University Press: New York, 1987.

(24) Zamir, E.; Levine, R. D. *Chem. Phys*. **1980**, *52*, 253.

(25) North, S. W.; Blank, D. A.; Gezelter, J. D.; Longfellow, C. A.; Lee, Y. T. *J. Chem. Phys.* **1995**, *102*, 4447.

(26) Gejo, T.; Takayanagi, M.; Kono, T.; Hanazaki, I. *Chem. Phys. Lett*. **1994**, *218*, 343.